Measurement of Receptor Concentration and Forward-Binding Rate Constant Via Radiopharmacokinetic Modeling of Technetium-99m-Galactosyl-Neoglycoalbumin

David R. Vera, Robert C. Stadalnik, Walter L. Trudeau, Paul O. Scheibe, and Kenneth A. Krohn*

Departments of Radiology and Internal Medicine, University of California, Davis, Medical Center, Sacramento, California

Technetium-99m-galactosyl-neoglycoalbumin (^{99m}Tc-NGA) is a synthetic ligand to the hepatocyte receptor, hepatic binding protein (HBP). A five-state mathematical model containing a bimolecular chemical reaction was utilized for quantitative estimation of the following physiologic and biochemical parameters: extrahepatic plasma volume V_e; hepatic plasma flow F and volume V_h; receptor-ligand forward-binding rate constant k_b and reaction volume V_r; and receptor concentration $[R]_o$. Nine normal subjects were studied. Given (a) liver and heart time-activity data, (b) the patient's weight, height, and hematocrit, (c) the fraction of injected dose in a 3-min blood sample, and (d) the amount and galactose density of the NGA dose, a computer program executed a curve-fit to the kinetic model. Systematic error, as measured by reduced chi-square, ranged from 1.43 to 2.56. Based on the nine imaging studies, the mean and relative error of each parameter were: $[R]_o$, 0.813 ± (0.11) μM; k_b, 2.25 ± (0.15) μM^{-1} min^{-1}; F, 0.896 ± (0.20) liter/min; V_e, 1.67 ± (0.27) liter; and V_h, 0.228 ± (0.22) liter. Two unique features of ^{99m}Tc-NGA radiopharmacokinetic systems permit the simultaneous estimates of receptor quantity, ligand affinity, and hepatic plasma flow. The first is the ability to administer a quantity of ligand capable of occupying a significant fraction of receptor; and the second is a simple model structure that conserves mass.

J Nucl Med 1991; 32:1169–1176

Receptor-binding radiopharmaceuticals provide an opportunity to carry out analytic measurements of a specific biochemical interaction within its native physiologic environment (*1,2*). The fundamental components that govern the rate of a receptor-binding process are the receptor and ligand concentration, and the forward and reverse binding rate constants. Various models have been tested for a variety of receptor-binding radiotracers: ^{18}F-spiroperidol (*3–5*), ^{11}C-*N*-methyl-spiperone (*6–8*), ^{11}C-quinuclidinyl benzilate methiodide (*9*), ^{11}C-raclopride (*10*), and ^{11}C-carfentanil (*11*). Each of these methods, however, suffer from a common deficiency: they cannot simultaneously measure an index of receptor affinity, such as the forward-binding rate constant k_b, and the concentration of receptor, $[R]_o$. This limitation results from an inability to safely inject an amount of ligand capable of occupying a significant fraction of free receptor.

We present here the kinetic analysis of a receptor-binding radiopharmaceutical, technetium-99m-galactosyl-neoglycoalbumin (^{99m}Tc-NGA), that permits high precision measurements of both k_b and $[R]_o$. This was achieved via optimization of the radiopharmacokinetic system (*12*) by using a ^{99m}Tc-NGA preparation of moderate affinity and injections of a high molar dose. We illustrate the analysis of ^{99m}Tc-NGA time-activity data using subjects with normal hepatic function.

MATERIALS AND METHODS

Human Subjects

Four female and five male subjects were studied. Their ages ranged from 26 to 42 yr and their weight ranged from 48 to 87 kg. Table 1 lists the age, sex, height, weight, hematocrit, expected plasma volume (*13*) and hepatic plasma flow (*14*), and the ^{99m}Tc-NGA dose of each study. Liver function tests, urine analysis, and cellular blood counts were performed within 24 hr prior to the ^{99m}Tc-NGA study and between 24 and 48 hr after the study. Each imaging study was performed in the morning after a 12-hr fast by the subject. All subjects had normal test values and had not received any medication within 2 wk prior to the ^{99m}Tc-NGA study. The protocol was approved by the University of California, Davis Human Subjects Review Committee. Informed consent from each subject was obtained prior to the ^{99m}Tc-NGA study.

Radiopharmaceutical Preparation

The NGA, having 24 galactose units per albumin molecule, was prepared by the covalent coupling of IME-thiogalactose to normal human serum albumin (*15*). The product was sterile and nonpyrogenic. Labeling of NGA with ^{99m}Tc was achieved by the electrolytic method (*15*). The final concentration of the labeled product was 5.2×10^{-5} *M*. Quality control was performed using high-performance liquid chromatography (TSK-3000SW, Beck-

Received Oct. 23, 1989; revision accepted Nov. 14, 1990.

For reprints contact: David R. Vera, PhD, Division of Nuclear Medicine, University of California, Davis, Medical Center, 2315 Stockton Blvd., Sacramento, CA 95817.

* Current address: Department of Radiology, University of Washington Medical Center, Seattle, WA.

TABLE 1
Human Subjects

Subject no.	Age (yr)	Sex	Height (m)	Weight (kg)	Hematocrit (%)	Expected plasma volume (liter)	Expected hepatic plasma flow (liter min^{-1})	Dose (mCi)
1	33	Male	1.70	75	42	2.80	1.00	4.5
2	29	Male	1.83	73	39	3.15	1.02	4.0
3	41	Male	1.75	70	41	2.86	0.95	4.9
4	27	Male	1.75	69	39	2.91	0.97	4.9
5	26	Male	1.73	66	44	2.57	0.85	6.2
6	30	Female	1.70	51	40	2.17	0.70	5.4
7	42	Female	1.50	48	46	1.60	0.60	4.1
8	39	Female	1.58	49	37	2.00	0.71	4.2
9	32	Female	1.75	87	41	2.92	1.18	4.9

man Instruments; Palo Alto, CA) (1.0 ml/min, 0.9% saline) with radioactivity (100–200 keV), and optical absorbance (280 nm) detectors. Last, a counting standard (0.1 ml polypropylene test tube), representing a 5000-fold serial dilution of the labeled product, was prepared and counted.

Data Acquisition

Each patient received an intravenous injection of ^{99m}Tc-NGA scaled to 1.8×10^{-9} mole per kilogram of body weight. Injected activity ranged from 4.0 to 6.2 mCi. Patients were imaged in the supine position under a large field of view gamma camera (ARC 3000, ADAC Laboratories, Milpitas, CA) fitted with a low-energy all-purpose parallel-hole collimator. A symmetric 15% window was employed. The center of the field of view was positioned over the xiphoid, which permitted visualization of the entire liver and heart. Computer (DPS 33000, ADAC Laboratories; Milpitas, CA) acquisition of gamma camera data was started just prior to injection of ^{99m}Tc-NGA. Digital images (128 × 128 pixels) were acquired in byte mode at a rate of four frames per minute. A timer was started when the bolus of activity entered the left ventricle of the heart. Three minutes later, approximately 1.0 ml of blood was drawn and transferred to a preweighed polypropylene test tube. Computer acquisition (256 × 256 × 16) was halted after 30 min, after which static images (1000K cts), including anterior, posterior, right lateral, and right anterior oblique views, were obtained.

The time-activity curves for the blood and liver were generated with the use of standard nuclear medicine software in the following manner. The frame representing an image acquired during 5.0–5.25 min postinjection was recalled for viewing. Regions of interest (ROIs) were then identified for the whole liver and heart, leaving sufficient space to differentiate between the two organs. Counts within each ROI were then calculated for each frame. The first frame of the dynamic study, and hence zero time, was identified by searching for the maximum counts within the heart ROI. Then, data from the liver and heart ROIs were normalized for counting time, and corrected for radioactive decay and background.

The fraction of injected NGA per liter of plasma, $\hat{I}$, was based on the subject's peripheral hematocrit, the weight of the 3-min blood sample (corrected by the specific gravity of whole blood; 1.05 mg/ml), and the radioactivity assay (100–200 keV) of the counting standard and blood sample.

The Kinetic Model

Figure 1 represents a schematic of the ^{99m}Tc-NGA kinetic model. The model can be divided into three sections: (a) the initial conditions, (b) the model states, and (c) the ROI time-activity data.

Initial Conditions. Each term above the top diagonal arrows represents an equation that equals $[L]_e$, $[L]_h$ and [D] at time t_s, the start of simulation. These terms are referred to as the initial conditions (Equation A2a–d of the Appendix) and are based on the fraction of injected dose per liter $\hat{I}$ at time t_s and assume conservation of NGA between liver and plasma. Initial conditions at time t_s rather than time zero are required because compartmental models assume instantaneous mixing within each compartment. We therefore sampled the plasma compartment at 3 min postinjection to allow homogenous distribution of ^{99m}Tc-NGA within the plasma.

Model States. The center line represents the exchange of ^{99m}Tc-NGA between extrahepatic and hepatic plasma and the bimolecular reaction of ^{99m}Tc-NGA with hepatic binding protein (HBP) at the hepatocellular membrane (see Equations A1a–d). Symbols for each state which are described in Table 2 are: $[L]_e$, $[L]_h$, [C], and [D]. The arrows within the center line represent the physiologic and chemical processes that control ^{99m}Tc-NGA uptake. These include hepatic plasma flow F, extrahepatic plasma volume V_e, hepatic plasma volume V_h, receptor concentration $[R]_o$, forward-binding rate constant k_b, and ligand-receptor reaction volume V_r.

ROI Data. Symbols $\hat{Y}_1$ and $\hat{Y}_2$ represent liver and heart ROI data which are coupled to the model states by detector sensitivity coefficients σ (see Equations A3a–b).

Parameter Estimation

Estimates of parameters $[R]_o$, F, k_b, V_e, V_h, and σ_1 proceeded in a two-step process. First, all model parameters were assigned initial values. Initial values for V_e and V_h in liters were calculated from total plasma volume, which was based on sex, total body weight, height (*13*), and peripheral hematocrit (see Appendix, Equations A4–A6). The calculation of hepatic plasma volume assumed 13% of the plasma volume in the liver, with 60% of the hepatic plasma volume within the sinusoids (*14*). The initial value for parameter $[R]_o$ was determined by the curvature of the liver time-activity data (Equation A7). The initial value for parameter F in liters per minute was based on peripheral hematocrit

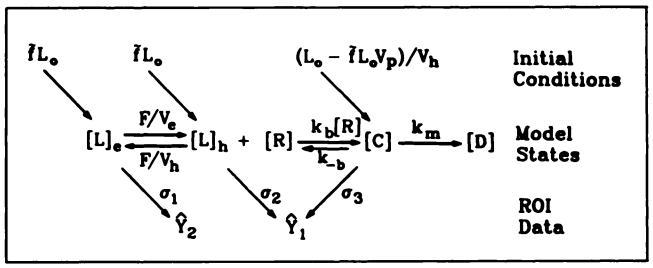

FIGURE 1. The kinetic model for ^{99m}Tc-NGA receptor binding uses a bimolecular chemical reaction. The objective of the kinetic analysis is the simultaneous estimation of parameters $[R]_o$, k_b, F, V_e, V_h, and σ_1. These parameters represent receptor concentration, ^{99m}Tc-NGA-receptor forward binding rate constant, hepatic plasma flow, extrahepatic plasma volume, hepatic sinusoidal plasma volume, and a detector sensitivity coefficient.

TABLE 2
Symbols

Symbols	Description	Units
[C]	ligand-receptor complex concentration	μM
[D]	lysosomal metabolite concentration	μM
F	hepatic plasma flow	liter min^{-1}
$\tilde{f}$	fraction of the injected Tc-NGA dose per liter	$liter^{-1}$
k_b	forward-binding rate constant	μM^{-1} min^{-1}
k_{-b}	reverse-binding rate constant	min^{-1}
k_m	metabolic rate constant	min^{-1}
$[L]_e$	NGA concentration in extra-hepatic plasma	μM
$[L]_h$	NGA concentration in hepatic plasma	μM
L_o	amount of NGA injected	μmol
n	total number of data points	
$[R]_o$	receptor concentration preinjection	μM
t_s	time of plasma sample and start of simulation	min
V_e	extra-hepatic plasma volume	liter
V_h	hepatic plasma volume	liter
V_r	reaction volume (assumed equal to V_h)	liter
V_p	total plasma volume (equal to $V_e + V_h$)	liter
$\hat{Y}_1$	simulated liver ROI count rate	cts min^{-1}
$\hat{Y}_2$	simulated heart ROI count rate	cts min^{-1}
Δt	frame duration	min
σ	detector sensitivity coefficient	cts min^{-1} nM^{-1}
χ^2_ν	reduced chi-square	

and total body weight (Equation A8). The initial value for parameter k_b in molar per minute was based on the NGA galactose density, ρ_{gal}, (*16*) (Equation A9). Based on in vitro measurements (*17*) of human tissue, the reverse-binding rate constant, k_b, was set equal to 3.3×10^{-4} min^{-1}. Parameter k_m was set to zero. The initial values for parameters σ_1 through σ_5 were based (Equations A10–A14) on the plasma sample, Y_2 and Y_1 at time t_s, and derived from Equation A3a and A3b using conservation of mass.

In the second step, solutions for the state equations (Equation A1) were calculated numerically (see Notes) (*18*) (VMS Version 4.7, Digital Equipment Corporation; Maynard, MA) for each time point starting at t_s. The liver ROI was simulated from t_s to the end of data acquisition. The heart ROI was simulated from t_s to 15 min postinjection. Initial conditions for the numerical solution were supplied by Equations A2a–d. Simulated values for the heart ($\hat{Y}_{2j}$) and liver ($\hat{Y}_{1j}$) time-activity data were generated by conversion of the model state to observational values via Equations A3a–b. Maintaining the constraints defined by Equations A2c, A3b, A12 and A14, parameters $[R]_o$, k_b, F, V_e, V_h, and σ_1 were adjusted until a minimum value for the weighted sum of squares, ss_w, (*19*) (Equation A15) was obtained. Minimization employed the downhill simplex algorithm (*20*). Boundary limits were imposed on the parameters F and V_h (2× normal value) during the curve-fit procedure. Termination was made when the fractional change in ss_w was less than 1.0×10^{-4}.

After termination of the curve-fit, systematic error (goodness-of-fit) was measured by reduced chi-square (*21*) (Equation A17). The variance-covariance matrix was calculated by singular value decomposition (*22*) of the system sensitivity matrix (*12*). The square root of each diagonal element of the covariance matrix was used as the standard error of parameter estimates $[R]_o$, k_b, F, V_e, V_h, and σ_1.

Model Predictions

The simulation was used to predict the relative values of each model state. The fraction of injected dose for NGA within the hepatic sinusoid f_{L_h}; extrahepatic plasma f_{L_e}; NGA-HBP complex f_c; metabolic product f_D; and free receptor f_R, were calculated (see Appendix).

RESULTS

Parameter Estimation

Table 3 lists the parameter estimates resulting from curve-fits to time-activity data of each ^{99m}Tc-NGA study. The parameters that were adjusted during the curve-fitting process, $[R]_o$, k_b, F, V_e, V_h, and σ_1, are tabulated as the estimated mean with relative standard error, se(p)/p. The fixed parameters, $\tilde{f}$ and L_o, were measured and assumed to be errorless. The parameters that were constrained during curve-fitting, σ_2, σ_3, and σ_4, are reported with relative standard errors. Systematic error listed in Table 3 as reduced chi-square χ^2_ν ranged from 1.43 to 2.56. Low values indicate low systematic error of the curve-fit. The study with the best fit to the liver observer was Subject 1. The worst fit was Subject 5. Curve fits to the liver observer employed approximately 105 points, whereas fits to the heart data used approximately 45 points. Table 4 contains the mean, $\bar{x}$, standard deviation, s.d., relative uncertainty, s.d./$\bar{x}$, and range of each model parameter.

The curve-fit to Subject 1 is illustrated in Figure 2. Triangles and diamonds represent decay-corrected count rates for the liver and heart ROIs. The smooth lines represent the $\hat{Y}_1$ and $\hat{Y}_2$ simulations of the ^{99m}Tc-NGA kinetic model. The curve-fit produced a receptor concentration $[R]_o$ of 0.914 ± (0.093) μM, k_b of 2.23 ± (0.28) μM^{-1} min^{-1}, and a hepatic plasma flow, F, of 0.685 ± (0.46) liter min^{-1}.

Model Predictions

The percent injected dose (%ID) (Fig. 3) calculated by the kinetic simulation predicted that 97% of the injected NGA existed as NGA-receptor complex C at 30 min. A plot of the percentage of free receptor (Fig. 4) versus time predicted that 50% of the total receptor existed as HBP-NGA complex at 30 min postinjection.

DISCUSSION

Radiopharmacokinetic modeling of ^{99m}Tc-NGA is the first in vivo radioassay to provide simultaneous estimates of receptor quantity and affinity with a single injection. Our design of ^{99m}Tc-NGA as an in vivo radioassay started with pre-experimental simulations (*12*), which predicted the requirement of high ^{99m}Tc-NGA affinity and molar dose for maximum precision of $[R]_o$ and k_b. Based on conservation of mass, the imposition of Equations A2c and A11 were employed to minimize the number of unknown parameters. The result is a quantitative technique that measures tissue function based on information contained within the shape of the time-activity curves.

TABLE 3
Parameter Estimation

Subject no.	Adjusted*						Measured		Constrained*		χ^2_ν
	$[R]_o$ (μM)	k_b (μM^{-1} min^{-1})	F (liter min^{-1})	V_c (liter)	V_h (liter)	σ_1 (cts min^{-1} nM^{-1})	$\bar{i}$ (liter^{-1})	L_o (μmole)	σ_2 and σ_3 (cts min^{-1} nM^{-1})	σ_4 and σ_5 (cts min^{-1} nM^{-1})	
1	0.914 ± (0.093)	2.23 ± (0.28)	0.685 ± (0.46)	1.99 ± (0.010)	0.274 ± (0.003)	1.58 ± (0.010)	0.184	0.136	0.517 ± (0.015)	0.070 ± (0.010)	1.43
2	0.893 ± (0.075)	2.12 ± (0.21)	0.936 ± (0.43)	2.36 ± (0.008)	0.294 ± (0.003)	2.34 ± (0.008)	0.172	0.133	0.627 ± (0.012)	0.097 ± (0.008)	1.63
3	0.863 ± (0.149)	1.70 ± (0.35)	0.813 ± (0.77)	2.10 ± (0.018)	0.287 ± (0.005)	2.59 ± (0.012)	0.147	0.136	0.457 ± (0.027)	0.121 ± (0.012)	2.13
4	0.700 ± (0.043)	2.40 ± (0.16)	1.224 ± (0.79)	1.77 ± (0.013)	0.229 ± (0.004)	1.97 ± (0.011)	0.226	0.126	0.693 ± (0.019)	0.063 ± (0.011)	1.71
5	0.945 ± (0.195)	2.12 ± (0.51)	0.671 ± (0.82)	1.78 ± (0.021)	0.250 ± (0.005)	2.10 ± (0.016)	0.220	0.120	0.696 ± (0.030)	0.098 ± (0.016)	2.56
6	0.794 ± (0.043)	2.09 ± (0.12)	0.916 ± (0.48)	1.30 ± (0.009)	0.187 ± (0.002)	1.91 ± (0.007)	0.296	0.093	0.958 ± (0.013)	0.084 ± (0.007)	1.56
7	0.752 ± (0.008)	2.19 ± (0.35)	0.822 ± (1.55)	1.03 ± (0.033)	0.165 ± (0.009)	1.08 ± (0.003)	0.303	0.088	0.568 ± (0.047)	0.058 ± (0.029)	1.52
8	0.722 ± (0.003)	2.43 ± (0.11)	0.906 ± (0.51)	1.23 ± (0.008)	0.161 ± (0.002)	1.84 ± (0.007)	0.348	0.089	0.531 ± (0.012)	0.072 ± (0.007)	1.50
9	0.734 ± (0.017)	2.95 ± (0.10)	1.087 ± (0.56)	1.46 ± (0.012)	0.211 ± (0.004)	0.91 ± (0.009)	0.300	0.159	0.321 ± (0.017)	0.033 ± (0.009)	1.54

* estimate ± (se(p)/p)

TABLE 4
Statistical Summary

	Parameters					
	$[R]_o$ (μM)	k_b (μM^{-1} min^{-1})	F (liter min^{-1})	V_e (liter)	V_h (liter)	V_p (liter)
$\bar{x}$*	0.813	2.24	0.896	1.67	0.228	1.89
sd(x)†	0.092	0.33	0.178	0.44	0.051	0.49
sd(x)/$\bar{x}$	0.11	0.15	0.20	0.27	0.22	0.26
min	0.700	1.70	0.671	1.03	0.161	1.20
max	0.945	2.95	1.224	2.36	0.294	2.65

* n=9
† standard deviation

Calibration of the time-activity data is achieved from a single plasma sample and does not require specialized tomographic gantries.

Radiopharmaceutical Preparation and Data Acquisition

Most receptor-binding radiopharmaceuticals are positron emitters and require specialized instrumentation such as a cyclotron and positron emission tomograph. Technetium-99m is a generator-produced radionuclide and its labeling to NGA can be achieved by direct labeling (*23*) or chelation (*24*) via stannous reduction. Data acquisition only requires standard nuclear medicine instrumentation and computer software and is completed within 45 min. Operationally, the kinetic analysis program starts by asking for five pieces of information: (a) the name of the file containing the time-activity data; (b) the patient's weight, height, and hematocrit; (c) the volume of ^{99m}Tc-NGA injected; (d) the time of the plasma sample (typically 3

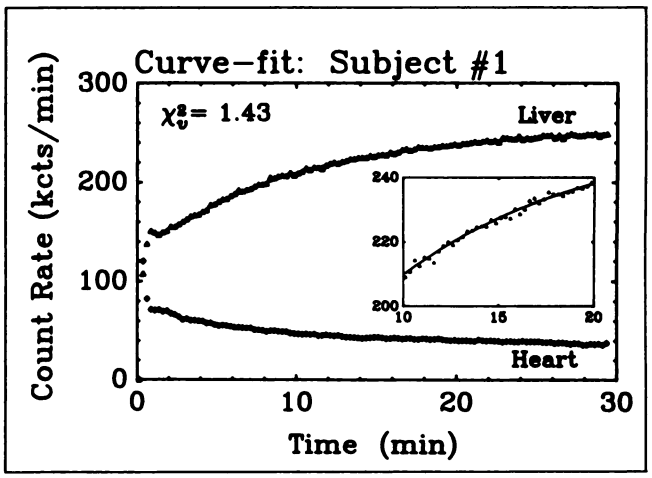

FIGURE 2. A curve-fit to Subject 1. Triangles and diamonds represent decay-corrected count rates for the liver and heart ROIs. The smooth lines represent $\hat{Y}_1$ and $\hat{Y}_2$, the kinetic simulations. The reduced chi-square χ^2_ν was 1.43. The fit produced a receptor concentration of 0.914 ± (0.093) μM and a forward binding rate constant of 2.23 ± (0.28) μM^{-1} min^{-1}. The insert shows the liver simulation and ROI data between 10 and 20 min postinjection.

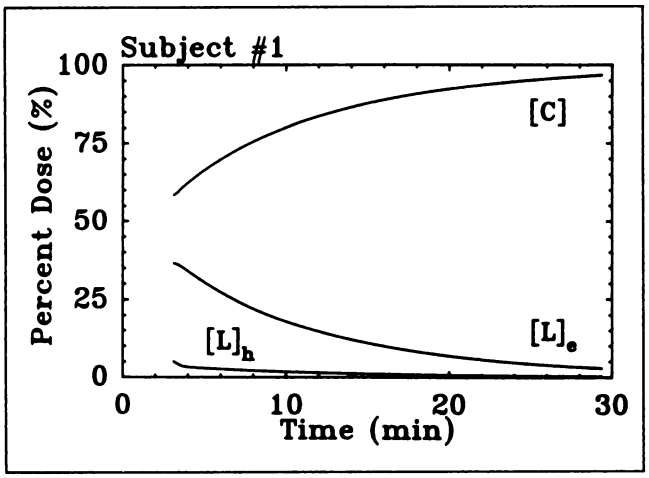

FIGURE 3. The %ID calculated by the kinetic simulation predicted that 97% of the injected NGA existed as NGA-receptor complex [C]. The sum of $[L]_h$ and [C] equals the percentage of NGA within the liver.

min); and (e) the fraction of ^{99m}Tc-NGA per liter of plasma in the counted sample. After this data has been entered, parameter estimation is completely automatic, including the generation of all statistical and graphic output. Moreover, the program executes on hardware common to many nuclear medicine computers.

The Kinetic Model

The most significant feature of a receptor-binding radiopharmaceutical as an analytic tool is the precision with which a mathematical model may be constructed. By incorporation of a bimolecular reaction that realistically describes the chemical kinetics of ligand binding to a receptor, the ^{99m}Tc-NGA model (*12*), as well as other brain (*3,5,7,11*) and myocardial (*9*) receptor models, are able to assign specific biochemical parameters to the process of tissue localization.

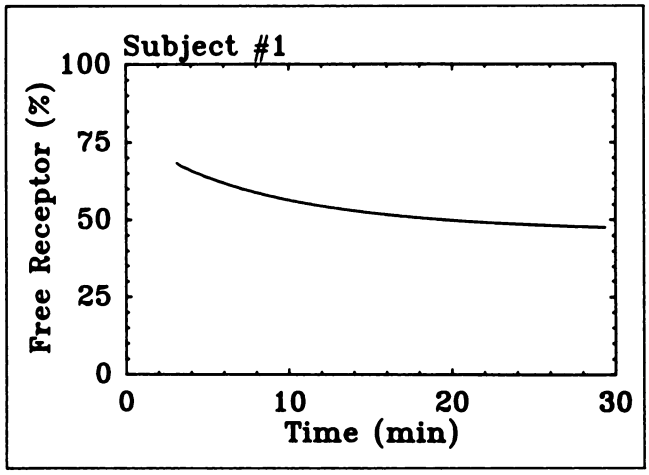

FIGURE 4. A plot of the free-receptor fraction versus time predicted that 50% of the total receptor existed as HBP-NGA complex at 30 min postinjection.

Five features provide ^{99m}Tc-NGA with significant advantages as a radiopharmaceutical for kinetic modeling of in vivo receptor biochemistry:

1. There is no barrier between hepatic plasma and receptor-bearing hepatocyte plasma membrane. This fact simplifies the kinetic model by permitting the removal of a hepatic intervascular compartment and its associated permeability-surface area constants.
2. We are able to safely inject an amount of NGA that will occupy a significant fraction of the receptor. This permits the ^{99m}Tc-NGA-receptor system to exhibit second-order kinetics (*25*) and, as a result, permits simultaneous estimation of $[R]_o$ and k_b (*12*).
3. Unlike the brain, the liver can be biopsied without harm to the subject. Consequently, the kinetic model can be validated by independent in vitro assays of tissue retrieved immediately after the imaging study.
4. Technetium-99m-NGA binding is highly irreversible (*16*). Consequently, ^{99m}Tc-NGA time-activity data are quite insensitive to the reverse-binding rate constant k_{-b} (*26*). As a result, we can neglect possible changes in k_{-b}.
5. Technetium-99m-NGA exhibits high cellular specificity. Galactosyl-neoglycoalbumin binds to the HBP protein receptor only, and this receptor is found only at the cell surface of hepatocytes. The result is twofold; extremely high localization by the liver (*16,26*), and the ability to impose conservation of mass within the kinetic model. The conservation of NGA between plasma and receptor-ligand complex permitted the constraints imposed by Equations A2.

In general, absolute quantification of imaging requires either an external standard to which the detection device is calibrated, or an internal standard. Receptor-binding radiopharmaceuticals, such as ^{99m}Tc-NGA, provide an internal mechanism, the bimolecular reaction, with which to standardize the measurement system. Three elements: (a) conservation of mass, (b) second-order operation of the system, and (c) knowledge of the injected amount, permit the absolute quantification of the hepatic receptor. Consequently, the amount (moles) of NGA injected is the standard to which the entire radiopharmacokinetic system is calibrated.

This model of NGA kinetics was designed for simplicity and compatibility with standard instrumentation. However, planar camera data without attenuation and scatter correction restricts the model to nonregional measurements. Therefore, the model parameters F and V_h must be interpreted as total values for the liver, and parameters k_b and $[R]_o$ as the average forward-binding rate constant and concentration of all receptors within the entire organ. Attempts to model flow and receptor heterogeneities will require a distributed/regional model structure (*27*) and a positron-emitting derivative of NGA, such as ^{68}Ga-deferoxamine-galactosyl-neoglycoalbumin.

Parameter Estimation

The primary goal of our kinetic modeling of ^{99m}Tc-NGA is the simultaneous measurement of receptor concentration and affinity, $[R]_o$ and k_b. Criteria for success is based on the magnitude of the relative errors associated with each parameter estimate. As a guide, parameter error should be small relative to the dispersion of the true parameter values within the patient or subject population. Based on this criterion, the precision of $[R]_o$ and k_b estimates are adequate. The relative standard error of the $[R]_o$ estimates (Table 3) ranged from 0.008 to 0.195 (median = 0.043) and was smaller than the relative standard deviation, $sd([R]_o)/[\bar{R}]_o$, of the nine subjects, 0.11 (Table 4). Similarly, the relative standard error of the k_b estimates ranged from 0.10 to 0.51 (median = 0.21) and was slightly larger than the relative standard deviation for k_b of the nine healthy subjects, 0.15.

A second issue is plausibility of the parameter estimates. Estimates of total plasma volume ($V_e + V_h$) and hepatic plasma flow, F, for each subject were similar to values predicted by standard formulas (*13,14*) (compare Tables 1 and 3).

Model Predictions

Simulations of the %ID within each compartment and percentage of free receptor are another means by which the curve-fitting procedure can be reviewed. One would look for unexpected predictions by the model, such as low %ID in ligand-receptor complex form at 20–30 min post-injection. If this prediction is made for a study that resulted in static images with normal ^{99m}Tc-NGA distribution (no heart activity), the parameters selected by the curve-fitting algorithm should be suspect and the curve-fitting procedure restarted. The plot of free receptor versus time is most useful in checking the parameter errors. Low relative errors (<10%) for parameters $[R]_o$ and k_b should correlate with large changes in the fraction of free receptor, R, during the 30-min study.

The free receptor plot for study 1 (Fig. 4) illustrates a feature of ^{99m}Tc-NGA that makes this radiopharmaceutical an exception to the current receptor-binding agents and, therefore, permits simultaneous estimation of parameters $[R]_o$ and k_b by the kinetic model. This feature is the ability to alter a significant amount of free receptor, [R], during the kinetic study. If [R] does not change during the image study, the term $\frac{k_b}{V_r}\{[R]_o - [C]\}$, which equals $\frac{k_b}{V_r}[R]$, within Equations A1b and A1c becomes a constant. The result is an inability to numerically distinguish k_b and $\{[R]_o - [C]\}$. Using the kinetic model under this condition produces estimates of $[R]_o$ and k_b with high standard errors (low precision). Therefore, low-specific activity injections of ^{99m}Tc-NGA permit a second-order response by the kinetic system and therefore make it sensitive to both receptor concentration $[R]_o$ and affinity k_b.

Operation of the radiopharmacokinetic system as a second-order process, however, requires careful balance between the requirements of high k_b and $[R]_o$ precision and high target-to-background. This is illustrated in Figure 3, which displays %ID simulations for the curve-fit to study 1. Simulation of the NGA-HBP complex C predicted a maximum uptake at 30 min of 97% of the ^{99m}Tc-NGA dose. This study produced $[R]_o$ and k_b estimates of moderate precision; the relative errors equaled 9.3% and 28%, respectively. If greater precision for $[R]_o$ and k_b is desired, a larger molar dose of ^{99m}Tc-NGA could be used. This however, would saturate the free receptor [R] during the study and result in lower hepatic uptake with less favorable imaging.

Significance

Estimates of kinetic parameters that represent receptor concentration and forward-binding rate constants can be obtained via mathematical modeling of ^{99m}Tc-NGA hepatocellular uptake. The next step in the modeling process is to compare parameters $[R]_o$ and k_b to independent measurements. If the model parameters correlate with or equal the measured values, the kinetic model can be employed as an analytic tool for investigation of in vivo receptor biochemistry. In vivo measurements or receptor biochemistry will be clinically efficacious only if receptor concentration of forward-binding rate constants are altered by disease. Therefore, the simultaneous estimation of $[R]_o$ and k_b represents the first of many stages toward clinical validation of a receptor-based radiopharmacokinetic model.

APPENDIX

This Appendix is divided into four parts. First, we present the state equations, initial conditions, and observation equations of the kinetic model. Second, we identify the equations by which the initial values of each model parameter are calculated. Third, we present the objective function with which we conducted the least squares fit of the model simulations of the detector data. Last, we present the calculation of the standardized residuals and the model predictions.

The Kinetic Model

The kinetic model (Fig. 1) exists as three sets of equations. The first set consists of the state equations.

$$\frac{d[L]_e}{dt} = \frac{F}{V_e}[L]_h - \frac{F}{V_e}[L]_e \qquad \text{Eq. A1a}$$

$$\frac{d[L]_h}{dt} = \frac{F}{V_h}[L]_e - \frac{F}{V_h}[L]_h - k_b[L_h]\{[R]_o - [C]\} + k_{-b}[C] \qquad \text{Eq. A1b}$$

$$\frac{d[C]}{dt} = k_b[L]_h\{[R]_o - [C]\} - k_m[C] - k_{-b}[C] \qquad \text{Eq. A1c}$$

$$\frac{d[D]}{dt} = k_m[C]. \qquad \text{Eq. A1d}$$

A second set, the initial conditions, provide a value for each state at time t_s, the start of simulation.

$$[L]_e(t_s) = \tilde{f}L_o \quad \text{Eq. A2a}$$

$$[L]_h(t_s) = \tilde{f}L_o \quad \text{Eq. A2b}$$

$$[C](t_s) = (L_o - \tilde{f}L_oV_p)/V_h \quad \text{Eq. A2c}$$

$$[D](t_s) = 0. \quad \text{Eq. A2d}$$

Equation A2c assumes conservation of mass and that the ligand-receptor reaction volume, V_r, is equivalent to the hepatic plasma volume, V_h. The third set comprises the observation equations and defines the coupling of the model states via detector sensitivity coefficients σ_1, σ_2, σ_3, σ_4, and σ_5 to the simulated liver and heart time-activity data, $\hat{Y}_1$ and $\hat{Y}_2$.

$$\hat{Y}_{1j} = \frac{1}{\Delta t_{1j}} \int_t^{t+\Delta t} (\sigma_2[L]_h + \sigma_3[C])dt \quad \text{Eq. A3a}$$

$$\hat{Y}_{2j} = \frac{1}{\Delta t_{2j}} \int_t^{t+\Delta t} (\sigma_1[L]_e + \sigma_4[L]_h + \sigma_5[C])dt. \quad \text{Eq. A3b}$$

Parameters σ_4 and σ_5 represent contamination of $\hat{Y}_2$ by liver activity and are a small fraction of σ_1.

Initial Parameter Values

The following equations were used to calculate initial values for each parameter.

$$TPV_m = (0.3669HT^3 + 0.03219TBW + 0.6041)(1\text{-}HCT/100) \quad \text{Eq. A4a}$$

$$TPV_f = (0.3561HT^3 + 0.03308TBW + 0.1833)(1\text{-}HCT/100) \quad \text{Eq. A4b}$$

$$lc = \frac{(Y_{1t_2} - Y_{1t_1})/12}{(Y_{1t_4} - Y_{1t_3})/8}, \quad \text{Eq. A4c}$$

where TPV_m and TPV_f are the total plasma volume for male and female subjects, respectively, and t_1, t_2, t_3, and t_4 are 3, 15, 20, and 28 min postinjection, respectively.

$$V_h = TPV\ 0.13 \times 0.6 \quad \text{Eq. A5}$$

$$V_e = TPV - V_h \quad \text{Eq. A6}$$

$$[R]_o = 0.70\ \mu M \text{ if } lc > 3.4 \quad \text{Eq. A7a}$$

$$[R]_o = 0.50\ \mu M \text{ if } 2.5 > lc > 3.4 \quad \text{Eq. A7b}$$

$$[R]_o = 0.35\ \mu M \text{ if } lc < 2.5 \quad \text{Eq. A7c}$$

$$F = TBW(1\text{-}HCT/100)\ 0.023\ l/min/kg \quad \text{Eq. A8}$$

$$k_b = \rho_{gal} 0.075\ \mu M^{-1}\ min^{-1} \quad \text{Eq. A9}$$

$$\sigma_1 = Y_{2t_4}/\tilde{f}L_o \quad \text{Eq. A10}$$

$$\sigma_2 = Y_{1t_s}V_h/(L_o - \tilde{f}L_oV_p) \quad \text{Eq. A11}$$

$$\sigma_3 = \sigma_2 \quad \text{Eq. A12}$$

$$\sigma_4 = 0.01\sigma_1 \quad \text{Eq. A13}$$

$$\sigma_5 = \sigma_4 \quad \text{Eq. A14}$$

Parameter Estimation

The weighted sum of squares equaled

$$SS_w = \sum_{i=1}^{2} \sum_{j=js}^{f} \frac{(Y_{ij} - \hat{Y}_{ij})^2}{V(Y_{ij})}, \quad \text{Eq. A15}$$

where js is the index of the starting frame, f is the index of the last frame of the i-th ROI, and $V(\hat{Y}_{ij})$ is the variance of the counting rate, $\hat{Y}_{ij}$, of the i-th ROI and the j-th frame. Based on a Poisson distribution for nuclear decay, the variance of Y_{ij} was defined as:

$$V(Y_{ij}) \equiv Y_{ij}/(\Delta T_{ij}). \quad \text{Eq. A16}$$

The reduced chi-square was calculated by

$$\chi_r^2 = SS_w/(N - P), \quad \text{Eq. A17}$$

where N is the number of data points used in the calculation of SS_w and equals the sum of the data points in each i-th ROI, and P is the number of parameters adjusted.

Model Predictions

The relative values of each model state were calculated as the fraction of injected dose f during the j-th time interval,

$$f_{L_ej} = [L]_{ej}V_e/L_o \quad \text{Eq. A18a}$$

$$f_{L_hj} = [L]_{hj}V_h/L_o \quad \text{Eq. A18b}$$

$$f_{cj} = [C]_jV_h/L_o \quad \text{Eq. A18c}$$

$$f_{D_j} = 1 - f_{L_ej} + f_{L_hj} + f_{cj} \quad \text{Eq. A18d}$$

$$f_{R_j} = ([R]_o - [C]_j)/[R]_o. \quad \text{Eq. A18e}$$

because all simulations used $k_m = 0.0$, f_D equaled zero.

NOTES

Interactive and batch-mode versions of the kinetic analysis program exist for the VAX computer running the VMS operating system (Digital Equipment Corp., Maynard, MA). The interactive version requires approximately 1 MByte of memory and supplies graphical output to the VAX-GPX workstation, or REGIS (VT240 and VT330 video terminals and the LA-100 graphics printer), HPGL (HP7550 pen plotter), and TEK4014 (LNO3 Plus laser printer) devices. In batch mode, parameter estimation, error analysis, and graphic output are completed within 5 min when executed on a VAX 3200. Version 6.0 of the program was used in this study.

ACKNOWLEDGMENTS

The authors thank Dr. William C. Eckelman for valuable discussions. We also acknowledge the excellent technical assistance of Dusan P. Hutak and R.L. Kennedy. We also thank ADAC Laboratories (Milpitas, CA) for the loan of a DPS-2200 image processing computer and VAX computer time during migration of the program to VMS from RT-11. This study was supported by U.S. Public Health Service grants RO1-AM34768 and RO1-AM34706, and U.S. Department of Energy grant DE-FG03-87ER60553.

REFERENCES

1. Kilbourn MR, Zalutsky MR. Research and clinical potential of receptor-based radiopharmaceuticals. *J Nucl Med* 1985;26:655–662.
2. Stadalnik RC, Vera DR, Krohn KA. Receptor-binding radiopharmaceuticals. Experimental and clinical aspects. In: Freeman LM, Weissmann HS,

eds. *Nuclear medicine annual 1986*. New York: Raven Press; 1986:105–139.
3. Mintun MA, Raichle ME, Kilbourn MR, Wooten GF, Welch MJ. A quantitative model for the in vivo assessment of drug-binding sites with positron emission tomography. *Ann Neurol* 1984;15:217–227.
4. Perlmutter JS, Larson KB, Raichle ME, et al. Strategies for in vivo measurement of receptor binding using positron emission tomography. *J Cereb Blood Flow Metab* 1986;6:154–169.
5. Logan J, Wolf AP, Shiue C-Y, Fowler JS. Kinetic modeling of receptor-ligand binding applied to position emission tomographic studies with neuroleptic tracers. *J Neurochem* 1987;48:73–83.
6. Wong DF, Wagner HN Jr, Dannals RF, et al. Effects of age on dopamine and serotonin receptors measured by positron tomography in the living human brain. *Science* 1984;226:1393–1396.
7. Wong DF, Gjedde A, Wagner HN Jr. Quantification of neuroreceptors in the living human brain. I. Irreversible binding of ligands. *J Cereb Blood Flow Metab* 1986;6:137–146.
8. Wong DF, Gjedde A, Wagner HN Jr, et al. Quantification of neuroreceptors in the living human brain. II. Inhibition studies of receptor density and affinity. *J Cereb Blood Flow Metab* 1986;6:147–153.
9. Syrota A, Comar D, Paillotin G, et al. Muscarinic cholinergic receptors in the human heart evidenced under physiological conditions by positron emission tomography. *Proc Natl Acad Sci USA* 1985;82:584–588.
10. Farde L, Hall H, Ehrin E, Sedvall G. Quantitative analysis of D2 dopamine receptor binding in the living human brain by PET. *Science* 1986;231:258–261.
11. Frost JJ, Douglass KH, Mayberg HS, et al. Multicompartmental analysis of [^{11}C]carfentanil binding to opiate receptors in humans measured by positron emission tomography. *J Cereb Blood Flow Metab* 1989;9:398–409.
12. Vera DR, Krohn KA, Scheibe PO, Stadalnik RC. Identifiability analysis of an in vivo receptor-binding radiopharmacokinetic system. *IEEE Trans Biomed Eng* 1985;BME-32:312–322.
13. Nadler SB, Hidalgo JU, Bloch T. Prediction of blood volume in normal adults. *Surgery* 1962;51:224–232.
14. Greenway CV, Stark RD. Hepatic vascular bed. *Physiol Rev* 1971;51:23–65.
15. Vera DR, Stadalnik RC, Krohn KA. [Tc-99m]galactosyl neoglycoalbumin: preparation and preclinical studies. *J Nucl Med* 1985;26:1157–1167.
16. Vera DR, Krohn KA, Stadalnik RC, Scheibe PO. [Tc-99m]galactosyl-neoglycoalbumin: in vitro characterization of receptor-mediated binding. *J Nucl Med* 1984;25:779–787.
17. Kudo M, Vera DR, Trudeau WL, Stadalnik RC. Validation of in vivo receptor measurements via in vitro radioassay: technetium-99m-galactosyl-neoglycoalbumin as a prototype model. *J Nucl Med* 1991;32:1177–1182.
18. Tendler JM, Bickart TA, Picel Z. A stiffly stable integration process using cyclic composite methods. *ACM Trans Math Software* 1978;4:339–368.
19. Carson ER, Cobelli C, Finkelstein L. *The mathematical modeling of metabolic and endocrine systems*. New York: John Wiley & Sons; 1983.
20. Nelder JA, Mead R. A simplex method for function minimization. *Computer Journal* 1965;7:308–313.
21. Bevington PR. *Data reduction and error analysis for the physical sciences*. New York: McGraw-Hill; 1969.
22. Press WH, Flannery BO, Teukolsky SA, Vetterling WT. *Numerical recipes: the art of scientific computing*. Cambridge: Cambridge University Press; 1986.
23. Kubota Y, Kojima M, Hazama H, et al. A new liver function test using the asialoglycoprotein-receptor system on the liver cell membrane. I. Evaluation of liver imaging using the Tc-99m-neoglycoprotein. *Jpn J Nucl Med* 1986;23:899–905.
24. Galli G, Maini CL, Orlando P, Deleide G, Valle G. A radiopharmaceutical for the study of the liver: ^{99m}Tc-DTPA-asialo-orosomucoid. I. Radiochemical and animal distribution studies. *J Nucl Med* 1988;32:110–116.
25. Vera DR, Krohn KA, Stadalnik RC, Scheibe PO. [Tc-99m]-galactosyl-neoglycoalbumin: in vivo characterization of receptor-mediated binding to hepatocytes. *Radiology* 1984;151:191–196.
26. Vera DR, Woodle ES, Stadalnik RC. Kinetic sensitivity of a receptor-binding radiopharmaceutical: technetium-99m-galactosyl-neoglycoalbumin. *J Nucl Med* 1989;30:1519–1530.
27. Bassingthwaighte JB, Goresky CA. Modeling in the analysis of solute and water exchange in the microvasculature. In: Renkin EM, Michel CC, eds. *Handbook of physiology, section 2: the cardiovascular system, volume 4, microcirculation, part 1*. Bethesda, MD: American Physiological Society; 1984:549–626.